PNAS RESEARCH ARTICLE | BIOPHYSICS AND COMPUTATIONAL BIOLOGY

All SNAP25 molecules in the vesicle–plasma membrane contact zone change conformation during vesicle priming

Ying Zhao[a,1], Qinghua Fang[a,1], Satyan Sharma[a,b], Shrutee Jakhanwal[c], Reinhard Jahn[c], and Manfred Lindau[a,d,2]

Edited by Axel Brunger, Stanford University, Stanford, CA; received June 6, 2023; accepted November 27, 2023

In neuronal cell types, vesicular exocytosis is governed by the SNARE (soluble NSF attachment receptor) complex consisting of synaptobrevin2, SNAP25, and syntaxin1. These proteins are required for vesicle priming and fusion. We generated an improved SNAP25-based SNARE COmplex Reporter (SCORE2) incorporating mCeruelan3 and Venus and overexpressed it in SNAP25 knockout embryonic mouse chromaffin cells. This construct rescues vesicle fusion with properties indistinguishable from fusion in wild-type cells. Combining electrochemical imaging of individual release events using electrochemical detector arrays with total internal reflection fluorescence resonance energy transfer (TIR-FRET) imaging reveals a rapid FRET increase preceding individual fusion events by 65 ms. The experiments are performed under conditions of a steady-state cycle of docking, priming, and fusion, and the delay suggests that the FRET change reflects tight docking and priming of the vesicle, followed by fusion after ~65 ms. Given the absence of wt SNAP25, SCORE2 allows determination of the number of molecules at fusion sites and the number that changes conformation. The number of SNAP25 molecules changing conformation in the priming step increases with vesicle size and SNAP25 density in the plasma membrane and equals the number of copies present in the vesicle–plasma membrane contact zone. We estimate that in wt cells, 6 to 7 copies of SNAP25 change conformation during the priming step.

exocytosis | transmitter release | vesicle fusion | SNAP25 | SNARE complex

Significance

Transmitter release and synaptic transmission are mediated by the neuronal SNARE (Soluble NSF Attachment REceptor) complexes. However, the number of copies of SNARE proteins that are cooperating in membrane fusion is currently unknown and controversial. We developed an improved SNAP25 (Synaptosomal-Associated Protein 25kDa)-based FRET construct that fully supports fusion in SNAP25 knockout embryonic mouse chromaffin cells. Combining electrochemical imaging of individual release events using electrochemical detector arrays with total internal reflection fluorescence resonance energy transfer (TIR-FRET) imaging, we detected a rapid FRET increase preceding individual fusion events by ~65 ms, indicating tight docking and priming. The number of copies that change conformation during this process involves all copies present in the vesicle–plasma contact zone.

The SNARE (Soluble NSF Attachment REceptor) complex, which in mammalian neurons and neuroendocrine cells is composed of the proteins synaptobrevin2 (Syb2 also called VAMP2), syntaxin 1 (Stx1), and SNAP25, plays a central role in docking and fusion of neurosecretory vesicles (1). The vesicular protein (v-SNARE) Syb2 is anchored in the vesicle membrane by a single transmembrane (TM) domain. The t-SNARE Stx1 is correspondingly anchored in the plasma membrane via a single TM helix. The third component, SNAP25 has lipid anchors in the plasma membrane. The SNARE complex is a core component of the fusion nanomachine, and conformational changes in one or more SNARE complexes are thought to be involved in various steps, from docking and priming to formation and dilation of fusion pores that allow for rapid transmitter release (2–5).

Synaptic vesicles contain ~70 copies of Syb2 (6), but it is controversial how many of these are acting together in the formation of a fusion pore (7). An imaging study suggested a minimal requirement of two copies for synaptic vesicle (SV) fusion (8). At least three copies of SNAP25 appear to be required for fast fusion in chromaffin cells (9). A very recent study showed 6 protein complexes, each presumably containing one SNARE complex as well as accessory proteins, arranged symmetrically connecting a "primed" SV to the plasma membrane (10). The number of Syb2 copies required for proteoliposome fusion was found to vary with vesicle size, suggesting a need for increased copy numbers with decreased membrane curvature (11). However, increased copy numbers may also be required to maintain the Syb2 density in the vesicle membrane. It has been suggested that the fusion rate may increase with increasing numbers of SNARE complexes and that activation of fusion within 1 ms may require a cluster of at least 15 SNARE complexes (12). In PC12 cells t-SNAREs form clusters consisting of 50 to 70 molecules (13, 14) and in INS1 cells of ~30 (15); in neurons, they consist of at least 10 but possibly many more (16). t-SNARE clusters may be associated with secretory granules but exist also elsewhere. In neurons, t-SNARE clusters showed a high level of colocalization between not only Stx1 and SNAP25 but also Munc18-1. In the absence of Stx1A and knockdown of Stx1B, the co-localization of SNAP25 with Munc18-1 was lost (16). A remarkable imaging study revealed that after tethering of a vesicle at the plasma membrane, the assembly of a Stx1/Munc18 cluster at this site is required to proceed to the docked state. Subsequently, on a time scale of 1 to 2 min, SNAP25 and Munc13 are recruited to the docking site (15), presumably preparing the vesicle for fusion in a priming step (17) such that the vesicle can be released rapidly in

Author contributions: Y.Z., Q.F., S.S., and M.L. designed research; Y.Z., Q.F., S.S., S.J., and M.L. performed research; Q.F. and S.S. contributed new reagents/analytic tools; Y.Z., Q.F., S.S., S.J., and M.L. analyzed data; M.L. developed software; and Y.Z., Q.F., S.S., R.J., and M.L. wrote the paper.

The authors declare no competing interest.

This article is a PNAS Direct Submission.

[1]Y.Z. and Q.F. contributed equally to this work.

[2]To whom correspondence may be addressed. Email: MXL2044@miami.edu.

This article contains supporting information online at https://www.pnas.org/lookup/suppl/doi:10.1073/pnas.2309161121/-/DCSupplemental.

Published January 3, 2024.

response to stimulation, i.e., Ca^{2+} entry via voltage-gated Ca^{2+} channels. It is possible that at this stage Munc13 entering the Stx1 cluster switches Stx1 to the open conformation and thereby recruits SNAP25 to the docking site. A recent super-resolution imaging study revealed that in presynaptic glutamatergic terminals, Munc13-1 forms multiple and discrete supramolecular self-assemblies that consist of at least 9 Munc13-1 copies stabilizing Stx1 clusters at the release sites (18).

Some of these studies provided estimates of the numbers of presynaptic proteins that are present at a release site but did not reveal how many of them actually participate in priming or fusion by exerting a conformational change. Using a SNAP25-based FRET (fluorescence resonance energy transfer) construct incorporating the fluorescent probes CFP and Venus at the N terminal ends of the SNAP25 SNARE domains as a SNARE COmplex REporter (SCORE) (19), we demonstrated a rapid conformational change in SNAP25 that is specifically associated with single fusion events (20). We now developed an improved version (SCORE2) incorporating mCerulean3 instead of CFP and show here that it is a fully functional substitute for wild-type SNAP25 in embryonal chromaffin cells from SNAP25 knock-out mice. Substituting SNAP25 with SCORE2 in cells devoid of wild-type SNAP25 allows estimation of the number of SCORE2 copies present at fusion sites and the fraction of them changing their conformation. The analysis indicates that in wt cells 6 to 7 copies of SNAP25 change conformation during the priming step, which precedes fusion by 65 ms.

Results

SCORE2 Fully Rescues Vesicle Release in $SNAP25^{-/-}$ Cells. In order to monitor conformational changes of the SNARE complex during vesicle fusion events in live cells, a SNAP25-based SCORE FRET probe named SCORE2 was generated. SCORE2 incorporates the FRET donor mCerulean3 and FRET acceptor Venus at the N termini of the two SNAP25 SNARE motifs SN1 and SN2, respectively. To test its functionality, SCORE2 was overexpressed in $SNAP25^{-/-}$ mouse embryonic chromaffin cells (E18), and fusion in response to depolarization pulses using a double-pulse protocol was assessed by whole cell patch clamp capacitance measurements (21). The averaged recordings of capacitance and calcium currents (I_{Ca}) from wild-type cells, $SNAP25^{-/-}$ cells, and $SNAP25^{-/-}$ cells overexpressing SCORE2 (from here on named SCORE2 cells) are shown in Fig. 1*A*.

The exocytotic responses, quantified as the average amplitudes of capacitance change induced by the 1st and 2nd pulse (Fig. 1*B*), were strongly reduced in $SNAP25^{-/-}$ cells (KO), compared to those from wild-type littermate control cells (wt) ($SNAP25^{-/-}$: 14.6 ± 1.5/11.3±1.9 fF, n = 17; control: 115.1 ± 22.7/22.6 ± 2.9 fF, n = 18; P = 0.00015/0.0028). The fusion deficiency in $SNAP25^{-/-}$ cells was fully restored by overexpressing SCORE2 (SC2) (SCORE2: 99.8 ± 7.2/26.3 ± 5.8 fF, n = 14; P = 0.57/0.54). Calcium currents were similar in all 3 cell types (Fig. 1*A*) and Ca^{2+} influxes, quantified as Ca^{2+} current charge integrals in response to 1st and 2nd pulse (Fig. 1*C*) were unchanged (control: 13.7 ± 2.6/11.8 ± 2.0 pC, $SNAP25^{-/-}$: 13.2 ± 1.3/10.1 ± 1.0 pC, P = 0.89/0.85; SCORE2: 12.2 ± 1.4/10.4 ± 1.3 pC, P = 0.95/0.65). The data in Fig. 1 indicate that SCORE2 is fully functional to support vesicle fusion in $SNAP25^{-/-}$ chromaffin cells.

SCORE2 Does Not Affect Frequency, Size, and Kinetics of Quantal Release Events. To test whether SCORE2-mediated quantal release events differ from quantal release events in wild-type cells, exocytosis was stimulated by extracellular high [K^+] and individual release events were detected by carbon fiber amperometry (Fig. 2*A*).

Consistent with the results of Fig. 1, the frequency of amperometric spikes was markedly reduced in $SNAP25^{-/-}$ cells but fully restored in SCORE2 cells (Fig. 2*B*, control: 60.4 ± 9.4 events/cell, n = 19; $SNAP25^{-/-}$: 3.6 ± 1.8 events/cell, n = 5, P = 0.006; SCORE2: 51.6 ± 7.9 events/cell, n = 16, P = 0.49). Amperometric spike parameters (Fig. 2*C*) were analyzed to determine whether quantal size and release kinetics of individual fusion events mediated by SCORE2 differ from those mediated by SNAP25 in control cells. Quantal size, the number of molecules released in a single fusion event, is obtained as the charge integral of the amperometric spikes and was not significantly different between SCORE2 mediated events (0.107 ± 0.008 pC) and control events (0.126 ± 0.012 pC, P = 0.21) (Fig. 2*D*). The amperometric spike kinetics was characterized by its amplitude (Fig. 2*E*) and half-width ($t_{1/2}$, Fig. 2*F*), which were also unchanged between SCORE2 cells and control cells (amplitude SCORE2/control: 23.4 ± 1.2/23.5 ± 1.1 pA, P = 0.97; $t_{1/2}$ SCORE2/control: 2.73 ± 0.23/3.01 ± 0.21 ms, P = 0.37).

The rapid amperometric spikes, reflecting the flux of transmitter from an expanded fusion pore, are often preceded by a small leakage current preceding the spike, called foot signal (22) (Fig. 2*C*), which reflects flux of transmitter through an initial narrow fusion pore (23, 24). Foot currents were characterized by their mean current amplitude (Fig. 2*C*, horizontal line) and duration, which indicate fusion pore structure and lifetime, respectively. These amperometric foot parameters (Fig. 2 *G* and *H*) were also not significantly different between SCORE2 cells and control cells (SCORE2/control: foot amplitude 2.74 ± 0.13/2.99 ± 0.12 pA, P = 0.16; foot duration

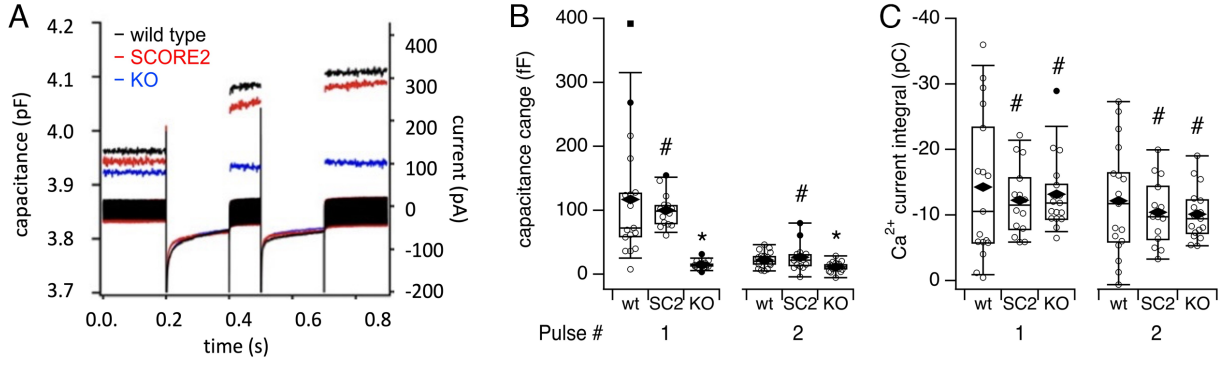

Fig. 1. SCORE2 fully rescues the release capability in $SNAP25^{-/-}$ embryonic mouse chromaffin cells. (*A*) Averaged I_{Ca} (right scale) and capacitance traces (left scale) in wt (black), $SNAP25^{-/-}$(blue), and SCORE2 (red) cells, which were stimulated by dual pulse depolarization (−70 to +10 mV, 200-ms pulse duration, and 100-ms inter-pulse interval). (*B* and *C*), Box plots of capacitance changes (*B*) and I_{Ca} integral (*C*) from individual cells in the 3 groups showing Tukey quartiles with whiskers at 9 and 91 percentiles, diamonds indicate mean values. *P < 0.01; #P > 0.05, compared to wt.

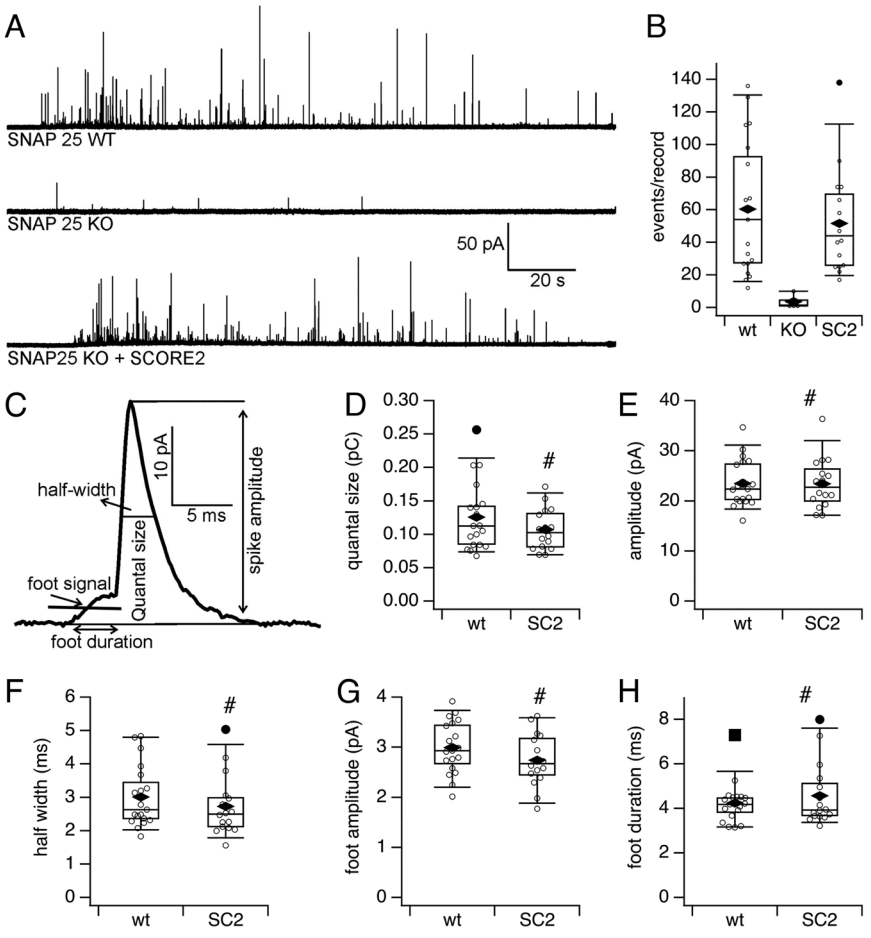

Fig. 2. SCORE2 restored vesicle release without modulating the kinetics of single fusion events. (*A*) Representative amperometric traces recorded from wt, SNAP25$^{-/-}$ and SCORE2 cells. (*B*) Box plot of number of amperometric spikes per cell in the respective groups. (*C*) Representative amperometric spike illustrating the determined spike parameters. (*D–H*) Box plots of median amperometric spike parameters in wt and SCORE2 (SC2) cells. In SNAP25$^{-/-}$ cells, numbers of spikes per cell were insufficient for statistical analysis. Box plots show Tukey quartiles with whiskers at 9 and 91 percentiles, diamonds indicate mean values *P < 0.01; #P > 0.05.

4.57 ± 0.35/4.24 ± 0.21 ms, P = 0.41). These results show that fusion events and fusion pore properties are unchanged when wild-type SNAP25 is replaced by SCORE2. SCORE2 is therefore fully functional as a SNAP25 replacement.

Density of SCORE2 Molecules at Vesicle Releasing Site. The full functionality of SCORE2 as a SNAP25 replacement makes it possible to quantitatively determine the number of SCORE2 (or SNAP25) proteins that change their conformation in a single fusion event. For this purpose, we performed electrochemical imaging (ECI) of single fusion events using electrochemical detector (ECD) arrays (25–27) combined with TIR (total internal reflection) FRET imaging, to detect and localize single fusion events and analyze fluorescence and its changes associated with these events (20). The ECD array consisting of 4 Pt electrodes (Fig. 3*A*) records fusion events as simultaneous amperometric spikes with the 4 electrodes, which detect different charge fractions and amplitudes, depending on the distance between the vesicle release site and the respective electrodes. By determining the fractional charge integral recorded from each of the 4 electrodes, the individual fusion event can be localized (27).

A SCORE2 cell was placed on top of the exposed ECD electrodes (Fig. 3*B*) and its footprint imaged in TIRF excitation mode using a 442-nm laser (Fig. 3*C*). The ECD traces from this cell are shown in Fig. 3*D*, and one example event is displayed on expanded scale in Fig. 3*E*. The location of this example event, as determined from the amperometric recording, is marked as a red dot in Fig. 3*C*. The fluorescence at the vesicle fusion site was quantified as the fluorescence of the 2 × 2 pixels 0.1-μm^2 area (159 nm/pixel) surrounding the fusion site. The mean sum of mCerulean3 fluorescence in these 4 pixels from 657 ECD fusion sites was 1,720 ± 52 CU (Camera Units). For calibration of single-molecule fluorescence, recombinant mCerulean3-SNAP25-His$_6$ molecules were generated and coupled to Ni-NTA (nickel-nitrilotriacetic acid) agarose beads at known densities. Using 442-nm TIRF excitation, as in cell experiments, a central area of the bead-coverslip contact zone was imaged and the average mCerulean3 intensity per pixel measured. Based on the known mCerulean3-SNAP25-His$_6$ density the fluorescence intensity per molecule was determined to be 3.38 CU per molecule (*Materials and Methods* section for details). Using this calibration, the average density of SCORE2 molecules at fusion sites was found to be ~510 (1,720/3.38 SCORE2 molecules per release site (defined as the 2 × 2 pixel area) or ~5,100 molecules/μm^2. As described in *Materials and Methods*, our quantification could possibly overestimate SCORE2 density by ~25%.

The density of overexpressed SCORE2 in SCORE2 cells was compared to that of SNAP25 in wild-type cells using immunofluorescence labeling, which showed that the labeling intensity in SCORE2 transfected cells was ~19-fold higher than that of endogenous SNAP25 in wt cells (wt: 650 ± 36 CU, n = 10; SCORE2: 12,338 ± 1,378 CU, n = 11, P < 0.01) (Fig. 3 *F* and *G*). This overexpression factor is in excellent agreement with that reported previously using the same transfection method (28). Based on these data, we estimate a SNAP25 density of ~270 molecules/μm^2 or ~27 molecules per 0.1-μm^2 release site in wild-type embryonal mouse chromaffin cells.

A SCORE2 FRET Change Specifically Associated with Fusion Events. Fluorescence emission in the mCerulean3 (467 to 499 nm) and Venus (520 to 550 nm) channels was tracked at the

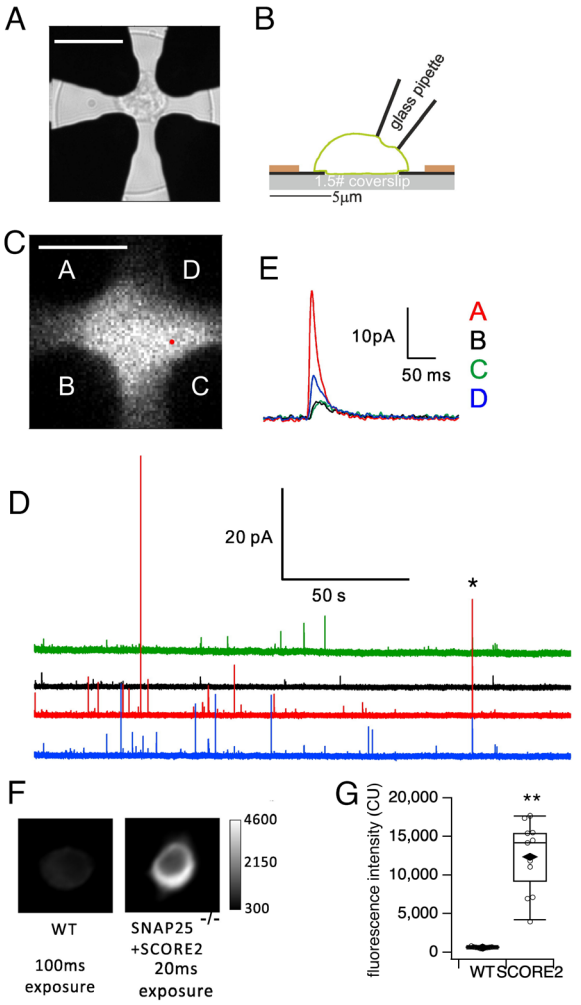

Fig. 3. Simultaneous ECI of single fusion events and TIRF imaging of SCORE2. (*A*) Bright-field image of ECD array. The four Pt electrodes are covered by a translucent insulation layer that is selectively removed within the circle region to expose the electrodes. A cell was placed at the ECD center contacting the electrode tips, (scale bar 10 μm.) (*B*) Schematic cross-sectional view of the ECD array illustrating the positioning glass pipette, cell (green outline), ECD insulation layer (brown), Pt electrodes (black), and #1.5 glass substrate (gray). (*C*) TIRF image of the footprint of a SCORE2 expressing cell placed on the ECD electrodes labeled with letters corresponding to the colors in *D* and *E*, (scale bar 5 μm.) (*D*) ECD recording traces. (*E*) The individual ECD event marked in d on expanded scale. (*F*) Immunofluorescence images of a wt cell and a SCORE2 cell. (*G*) Averaged fluorescence intensity of individual cells after background subtraction in wt and SCORE2 transfected SNAP25$^{-/-}$ cells. $^{**}P < 0.01$.

vesicle releasing sites in SCORE2 cells. The FRET analysis of single events suffers from poor signal-to-noise ratio (SNR). To improve SNR, the fluorescence intensity time course of each 6 × 6 pixel region surrounding the individual fusion site was therefore synchronized with respect to the amperometric spike start time. The averaged image sequences from 657 ECD events (Fig. 4) centered around the fusion sites show increased total fluorescence at the fusion site with no change associated with fusion (Fig. 4 *A*, *Top*) and an increase in FRET ratio at the fusion site at the time of fusion (Fig. 4 *A*, *Bottom*). The time of fusion (t = 0) is indicated by the averaged amperometric spike (Fig. 4*B*, green). The averaged time course of fluorescence in the central 4 pixels surrounding the fusion sites shows an abrupt increase in the acceptor channel (Venus, Fig. 4*B*, yellow) and a concurrent decrease with similar amplitude in the donor channel (mCerulean3, Fig. 4*B*, cyan) at the time of fusion, with ~12% increase of the intensity ratio (from here also called FRET ratio) (Fig. 4*B*, black). The FRET ratio remained at a plateau for ~1 s, followed by a gradual decline to the pre-fusion baseline level over next ~2 s. The result indicates a clear correlation between FRET increase and fusion events recorded by ECD amperometry.

The time resolution of the amperometric spikes reported by the ECD events is 1 ms. Due to low SNR of the fluorescence images, however, imaging frame durations of ~100 ms are needed to collect sufficient signal photons such that the precise temporal correlation of the FRET change with the time of fusion pore formation is uncertain. To obtain a more precise time correlation, we developed the Event COrrelation Microscopy (ECOM) method to analyze imaging signals with sub-frame time super-resolution (20, 29). In brief, we padded the frame intensities with 1-ms time points, assigning the same frame intensity to all the points within that frame. This makes it possible to align the imaging data at the onset of the amperometric ECD spikes with 1-ms precision such that the frames from different recordings can be temporally aligned with the respective amperometric spikes with sub-frame resolution. The aligned padded traces are averaged providing the averaged FRET

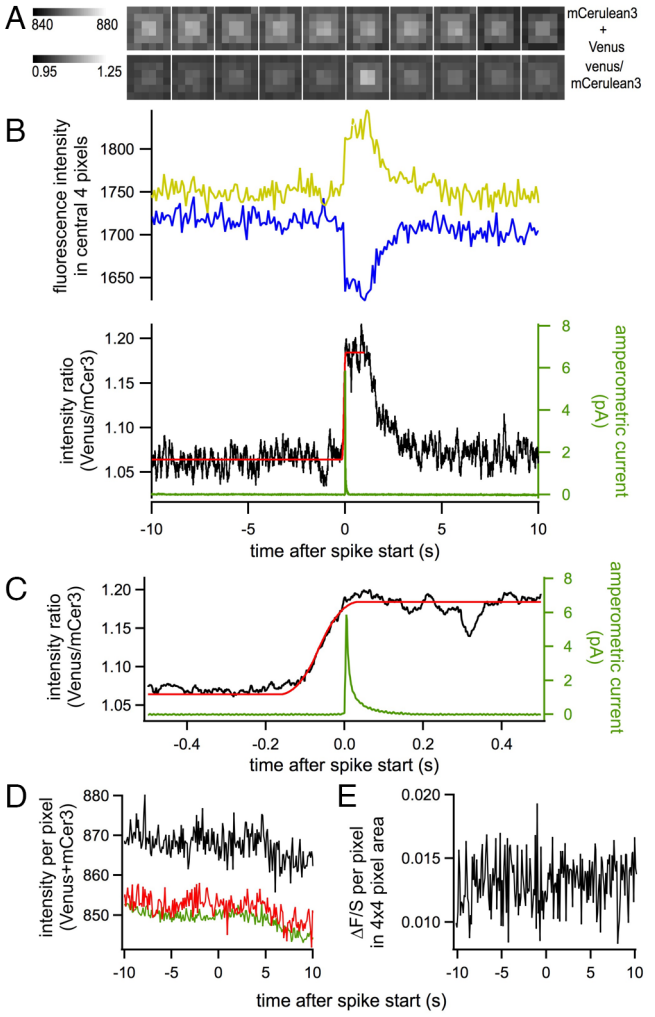

Fig. 4. FRET change precedes fusion pore opening. (*A*) Image sequence of averaged six-by-six-pixel regions centered at the release sites; (*Top*) total fluorescence mCerulean3+Venus; (*Bottom*) Venus/mCerulean3 ratio. (*B*) Averaged time course of mCerulean3 (blue), Venus (yellow) emission, and Venus/mCerulean3 ratio (black) at the release sites (2 × 2 pixels). (*C*) Venus/mCerulean3 ratio time course (black) analyzed with the ECOM method (29) on expanded scale, and fitted with the step response function (red). The green trace in *B* and *C* is the averaged amperometric trace obtained after temporal alignment of the traces at the spike start times. (*D*) Time courses of total fluorescence per pixel (mCerulean3+Venus) in the central 4 pixels (black), the peripheral 20 pixels of the 6 × 6 pixel area (red) and average of whole cell footprint (green). (*E*) Time course of ΔF/S. All data are averages of 657 events.

time course (Fig. 4*C*, black), representing the average time course of the FRET change lowpass filtered by the imaging frame integration time. For a stepwise change, the time where the change occurred is precisely indicated by the time of the half-maximal increase (29). Fitting the data of Fig. 4*C* with the ECOM step response function (29) (Fig. 4*C*, red) revealed that the SCORE2 FRET change precedes the fusion event by 65 ± 11 ms. In contrast to the FRET ratio, the sum of donor and acceptor fluorescence was unchanged before and after the fusion except for a small gradual decrease presumably due to bleaching (Fig. 4*D*, black).

The fluorescence intensity per pixel at the 2 × 2 pixel fusion sites (Fig. 4*D*, black) was 1.85% higher than that at the peripheral 20 pixels (Fig. 4*D*, red), which was similar to that averaged over the entire cell footprint (Fig. 4*D*, green). The average SCORE2 density in the peripheral 20 pixels is therefore reduced to ~5,000 copies per μm^2, compared to ~5,100 copies per μm^2 at the fusion sites. The extra fluorescence ΔF indicates the existence of vesicle-associated SCORE2 clusters at the fusion sites and extends over a 4 × 4 pixel (16 pixel) area (Fig. 4*A*) and was therefore defined as the difference between fluorescence intensities per pixel in the central 4 × 4 pixels surrounding the fusion site (F) and the fluorescence intensities per pixel in the peripheral 20 pixels (S), ΔF = F–S. Here, S is attributed to SCORE2 fluorescence that is spatially unrelated to fusion sites. The ratio ΔF/S is ~0.014 ± 0.002 (Fig. 4*E*) and shows no detectable changes related to the fusion process, indicating that the SCORE2 clusters do not immediately disperse after fusion from the vesicle releasing site, consistent with previous results (15, 20). With 5,000 copies per μm^2 in the periphery, the value of ΔF/S ~0.014 ± 0.002 in the 16 pixel (0.4 μm^2) area corresponds to 28 ± 4 extra copies in the cluster, consistent with previous estimates in PC12 cells and INS1 cells (14, 15).

The FRET Efficiency of SCORE2 Indicates SNARE Complex Formation. The FRET ratios were further analyzed to estimate the corresponding apparent FRET efficiencies. The FRET ratio R can be expressed as a simplified function of FRET efficiency E (20):

$$R = \frac{I_Y}{I_C} = A + B \bullet \frac{E}{1 - E}. \quad [1]$$

The coefficients A and B depend on experimental parameters such as excitation and emission efficiencies of the fluorophores and light collection efficiencies in the respective filter bands (20). To determine the apparent FRET efficiency of SCORE2 in the plasma membrane, acceptor photobleaching experiments were performed. The SCORE2 molecules in the membrane were alternately excited for 100 ms at 442 nm in TIRF mode acquiring the FRET images, and for 1 s in epifluorescence lamp excitation mode using a 510/20-nm bandpath filter for acceptor photobleaching. The acceptor photobleaching led to an intensity decrease of Venus and a concomitant increase of mCerulean3 (Fig. 5 *A*, *Left*). The increase in the mCerulean3 channel indicates a basal FRET efficiency E_{low} of ~21%. The average basal FRET ratio over the cells' footprints was R_{low} = 1.01.

Given the 19-fold overexpression factor (Fig. 3*G*) in cells overexpressing SCORE2, most of the SCORE2 will not be in a complex with Stx1 or Syb2. To obtain the FRET efficiency of SCORE2 in complex with Stx1, Stx1-mCherry and SCORE2 were co-expressed in $SNAP25^{-/-}$ cells. In these cells, we intentionally overexpressed more syntaxin than SCORE2 by introducing an internal ribosome entry site (IRES) in the Semliki Forest Virus (pSFV) construct and arranging the DNA fragment of Stx1-mCherry upstream IRES and SCORE2 downstream. To quantify the protein ratios of Stx1-mCherry/SCORE2, fluorescence imaging was performed. Venus of SCORE2 and mCherry were excited in epifluorescence mode using 510/10 and 561/14 filters (Semrock), respectively. The incident light intensities after passing through these filters were 152 mW and 479 mW for Venus and mCherry excitation, respectively. Fluorescence images were acquired with 535/30-nm and 594-nm long-pass emission filters for Venus and mCherry, respectively. Taking into account the transmission curves of the filters, spectral band collection efficiencies, and quantum yields (Venus 0.57; mCherry 0.22), a constant intensity ratio for equimolar densities of mCherry vs. Venus fluorophores was estimated as 1.46. Based on this conversion, acceptor photobleaching experiments were performed in selected cells that overexpressed ~10 times more Stx1 than SCORE2. This overexpression procedure allowed most of SCORE2 to be in a complex with 2 syntaxins. As shown in Fig. 5 *A*, *Right*, the apparent FRET efficiency under these conditions E_{high} was estimated to be ~38%.

The FRET ratio over the cell's footprint was R_{high} = 1.85. Based on these acceptor photobleaching experiments, the coefficients in Eq. **1** were estimated to be A ~ 0.38 and B ~ 2.4 and the apparent FRET efficiencies *E* can be calculated from the FRET ratios *R* as

$$E = (R - A) / (R + B - A). \quad [2]$$

To provide a realistic model of the structural changes leading to the observed FRET increase, we performed coarse-grained molecular dynamics simulations of uncomplexed SCORE2 alone in the membrane (Fig. 5 *B*, *Left*) and of SCORE2 incorporated into the ternary SNARE complex (Fig. 5 *B*, *Right*). In these simulations, we tracked the distance and κ^2 orientation factor between the FRET donor and acceptor and the resulting FRET efficiency (*SI Appendix*, Fig. S3). The mCerulean3 and mVenus incorporated in SCORE2 show slow tumbling motion such that the use of the "dynamic average" κ^2 = 2/3 is not justified. In the trajectories of these simulations, we identified states (Fig. 5*B*) with FRET efficiencies that match the experimentally observed values, These states exemplify how the transition from uncomplexed SCORE2 to SCORE2 incorporated in the SNARE complex may lead to the observed FRET increase. We note that due to the motions of the fluorescent proteins, the snapshots shown should be considered examples and that a detailed quantitative statistical analysis of the FRET values in such simulations will require extensive further investigation.

SCORE2 in Binary or Ternary SNARE Complex Exhibits Similar In Vitro FRET Efficiencies. In cells where the amount of syntaxin was 10-fold higher than SCORE2 most of SCORE2 presumably formed complexes with 2 Stx1 copies, instead of forming a ternary SNARE complex with Stx1 and Syb2. To determine whether the SCORE2 FRET state in the ternary SNARE complex is similar to that in a binary t-SNARE complex, we performed in vitro experiments to quantitatively estimate FRET efficiencies of SCORE2 under different conditions by the ExEm method (30). This method removes donor spectral bleed-through and acceptor cross excitation by simultaneously unmixing the excitation and emission spectra. According to this method, four spectra S^D (reference spectrum 1), S^A (reference spectrum 2), S^{DA} (FRET spectrum), and B (background spectrum), were generated on the basis of fluorescence intensity recorded in a range of excitation and emission wavelengths. S^D and S^A were generated in the presence of donor mCerulean3 only or acceptor Venus only, respectively (Fig. 5 *C*, *Left*). S^{DA} was generated in the presence of both mCerulean3 and Venus (Fig. 5 *C*, *Middle* and *Right*), and B was generated under blank condition. After removing background from each spectrum and normalizing the reference spectrum with corresponding fluorophore quantum yield, a reference sensitized

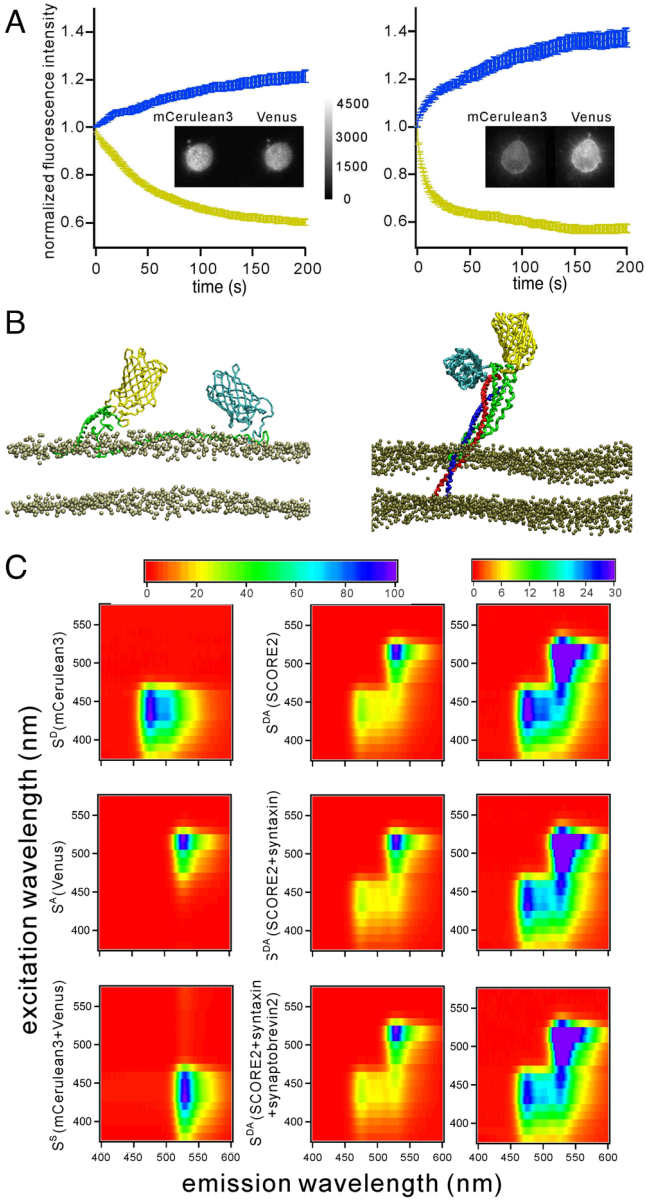

Fig. 5. The SCORE2 FRET efficiencies determined in live cells by photobleaching experiments or by in vitro experiments. (*A*) Photobleaching experiments were performed in embryonic mouse chromaffin cells overexpressing SCORE2 alone (*Left*) or co-expressing SCORE2 and excess Stx1-mCherry (*Right*). The cells were alternately exposed to epifluorescence lamp excitation at 500 to 520 nm to bleach the FRET acceptor Venus and were excited for 100 ms at 442 nm in laser TIRF mode while images were acquired. Intensities of Venus and mCerulean3 recorded from individual cells were normalized to the respective values before bleaching and averaged. The *Insets* show initial fluorescence images of cells before bleaching. The increase in the mCerulean3 channel indicates an averaged basal FRET efficiency of 21% (*Left*, n = 22), and high FRET efficiency in the presence of excess Stx1 of 38% (*Right*, n = 27). (*B*) Snapshots from coarse-grained molecular dynamics simulation of SCORE2 alone (*Left*, calculated FRET efficiency 0.2) and SCORE2 in ternary SNARE complex (*Right*, calculated FRET efficiency 0.39). (*C*) The in vitro FRET efficiencies of SCORE2 under different conditions were quantitatively estimated by the ExEm method simultaneously un-mixing the excitation and emission spectra collected on a spectrofluorometer. (*Left*) the reference spectra for donor mCerulean3 only (*Upper*, S^D), for acceptor Venus only (*Middle*, S^A), and for the sensitized emission spectrum (*Bottom*, S^S) obtained from convoluting the donor-only and acceptor-only spectra. (*Middle*) FRET spectrum for SCORE2 only (*Upper*, S^{DA}_{SCORE2}), for the mixture of SCORE2 and Stx1 (*Middle*, $S^{DA}_{SCORE2+Stx1}$), and for the mixture of SCORE2, Stx1 and Syb2 (*Bottom*, $S^{DA}_{SCORE2+Stx1+Syb2}$). (*Right*) the *Middle* panel displayed on an expanded intensity scale.

emission S^S was generated by combining normalized S^D and S^A, using the relation $S^{DA} = dS^D + aS^A + fS^S + bB$. The S^{DA} was deconvoluted to obtain the factors a, d, and f, which best satisfied the equation. The FRET efficiency *E* of SCORE2 in the absence of other SNARE proteins was calculated as ~0.138 ± 0.003 by E = f/(d + f). In the presence of either 10-fold excess Stx1 or 10-fold excess (Stx1+Syb2), the $S^{DA}_{syntaxin}$ and $S^{DA}_{syntaxin+syb2}$ were created following the same procedure, giving the calculated $E^{DA}_{syntaxin}$ and $E^{DA}_{syntaxin+syb2}$, 0.228 ± 0.005 and 0.242 ± 0.004, respectively. The calculated FRET efficiencies in complexes with Stx1 or with Stx1+Syb2 are therefore similar, indicating that the FRET state of SCORE2 in the t-SNARE complex with syntaxin reflects its conformation in the full ternary SNARE complex.

Estimating the Number of SCORE2 Molecules Undergoing a Conformational Change Preceding Fusion. The averaged pre- and post-fusion FRET ratios at the fusion sites (Fig. 4*C*) were averaged over 1 s before and 1 s after fusion, respectively, to estimate the number of SCORE2 molecules changing conformation preceding a fusion event. Using Eq. **2** and the parameter values A = 0.38 and B = 2.4, the apparent FRET efficiencies for the average $R_{pre\text{-}fusion}$ of 1.066 and $R_{post\text{-}fusion}$ of 1.184 can be calculated giving $E_{pre\text{-}fusion}$ = 0.222 and $E_{post\text{-}fusion}$ = 0.251, indicating that the average apparent FRET efficiency increased during vesicle fusion. If we assume that the different apparent FRET efficiencies reflect different relative numbers of SCORE2 molecules in two distinct FRET states and that a fraction α of molecules exhibit high FRET efficiency (E_{high}), whereas the remaining molecules show low FRET efficiency (E_{low}), the fluorescence intensity ratio becomes (20)

$$R = \frac{I_Y}{I_C} = A + B \bullet \frac{E_{low} + \alpha \bullet \left(E_{high} - E_{low}\right)}{1 - \left[E_{low} + \alpha \bullet \left(E_{high} - E_{low}\right)\right]}. \quad [3]$$

Comparing Eq. **3** to Eq. **1**, it can be seen that the apparent FRET efficiency corresponds to the expression $E_{app} = E_{low} + \alpha \bullet \left(E_{high} - E_{low}\right)$, and α can be calculated as

$$\alpha = \frac{E_{app} - E_{low}}{E_{high} - E_{low}}. \quad [4]$$

In cells overexpressing SCORE2, most of the SCORE2 is not in a complex with Stx1. Therefore, we assign the FRET efficiency (E = 0.213) determined by acceptor photobleaching as E_{low}. When excess Stx1-mCherry was co-expressed with SCORE2, the FRET ratio approached a value R = 1.85 (Fig. 5 *A*, *Right*) giving a calculated E_{high} = 0.382. According to Eq. **4**, pre- and post-fusion FRET efficiencies of 0.222 and 0.251 correspond to α values of 0.07 and 0.24, suggesting that a fraction Δα=17±1 % of the SCORE2 molecules in the 2 × 2 pixel area surrounding the fusion site undergo a conformational transition from the low FRET state to the high FRET state before fusion. With ~510 SCORE2 molecules present in this area at typical overexpression levels, this corresponds to ~87 molecules.

Fusion of Larger Vesicles Involves More SCORE2 Molecules Undergoing a Conformational Change. The actual number of SNARE copies required for vesicle fusion may depend on vesicle size. To modulate vesicle size, cells were pre-loaded with L-Dopa before combined ECD/TIR-FRET experiments were performed (Fig. 6). L-Dopa loading increases vesicle quantal size in parallel with vesicle volume without modifying the intravesicular transmitter concentration (31, 32). The analysis of fusion events in L-Dopa-treated cells showed again the existence of extra

fluorescence at the fusion sites (Fig. 6 *A*, *Top*). The ratio ΔF/S was 0.016 ± 0.002, not significantly different from that in the untreated cells. The FRET change was also similar (Fig. 6 *B* and *C*) and ECOM analysis (red fit lines in Fig. 6 *B* and *C*) revealed that in spite of larger vesicle size, the delay between the FRET change and fusion fore opening was 54 ± 8 ms, (Fig. 6*C*), not significantly different from that in control cells.

Compared to control vesicles, the L-Dopa-pre-loaded vesicles exhibited 1.68-fold larger quantal size Q (Fig. 6*D*, Control 0.112 ± 0.003 pC, L-Dopa 0.188 ± 0.005pC, $P < 0.001$). The averaged $Q^{1/3}$ values increased by 21%, Control: 0.455 ± 0.004 $pC^{1/3}$, L-Dopa 0.550 ± 0.004 $pC^{1/3}$, $P < 0.001$), suggesting a 21% increase of mean vesicle radius from 65 nm in control cells (33) to 78 nm in L-Dopa-treated cells (Fig. 6*E*). The averaged SCORE2 density in the central 4 pixels at the releasing sites of the L-Dopa-treated cells was 1,800 ± 35 CU, indistinguishable from that of control cells (1,720 ± 51 CU) (Fig. 6 *A* and *F*). Based on the FRET analysis of fusion events in the L-Dopa-treated cells, the estimated fraction Δα changing from the low FRET to the high FRET state was 20.2 ± 0.4 % (~100 SCORE2 molecules), which was significantly higher than that in untreated cells (17.0 ± 0.5 %, $P < 0.001$) (Fig. 6*G*).

Number of SCORE2 Copies Changing Conformation before Fusion Increases with Vesicle Size and SCORE2 Density. To analyze the fraction Δα of SCORE2 molecules that change their conformation as a function of vesicle size and of SCORE2 density at the release site, the Δα values were determined for each individual fusion event (n = 1,328, pooled from untreated and L-Dopa treated) from the pre- and post-fusion FRET ratios as described above for the average FRET ratio and sorted according to the cube root of quantal sizes, which is proportional to vesicle radius. The sorted events were successively sub-grouped in quartiles and the averaged Δα values of individual in each quartile plotted vs. their respective mean quantal sizes in the quartiles (Fig. 7*A*, red), revealing a positive correlation between Δα and vesicle size. Taking into account the slight decrease in SCORE2 density at very large vesicles (Fig. 7*A*, blue), the average numbers of SCORE2 copies changing conformation were calculated and plotted as a function of vesicle radius (Fig. 7*B*) showing a linear increase.

In Wild-Type Cells ~6-7 SNAP25 Molecules Undergo a Conformational Change before Fusion. In wild-type cells, SNAP25 is expressed with 19-fold lower density compared to SCORE2 overexpression. To estimate the predicted fraction $\Delta\alpha_{endogenous}$ of SNAP25 molecules that change their conformational state in wt cells, the Δα values for each individual fusion event were plotted vs. corresponding initial mCerulean3 intensities at the release sites (Fig. 7*C*). Due to the low SNR of individual events, the points scatter widely and could be fitted either linearly (blue line) or exponentially (red line). In wild-type cells, we estimate 27 SNAP25 molecules in the central 4 pixel area. Replacing these with 27 SCORE2 copies would give a total intensity of 90 CU. Extrapolating the fits to this value gives estimates of $\Delta\alpha_{endogenous}$ values of 0.24 and 0.26 for linear and exponential fits, respectively (green arrows). To filter the noise, the events were sorted according to the mCerulean3 intensity at the releasing sites and successively sub-grouped by quartile. The mean Δα values of these quartiles increase with decreasing mean mCerulean3 intensities of the respective quartiles (Fig. 7*D*). Averaged traces of the low quartile and high quartile groups indicate that in the high quartile group ~4% of SCORE2 copies are in the high FRET state before fusion, and that this fraction increases to 18% after fusion, while in the low quartile group, 28% are in the high FRET state before fusion and that this fraction increases to 54% after fusion (*SI Appendix*, Fig. S1 *A* and *B*). The Δα value thus increases from 14% in the

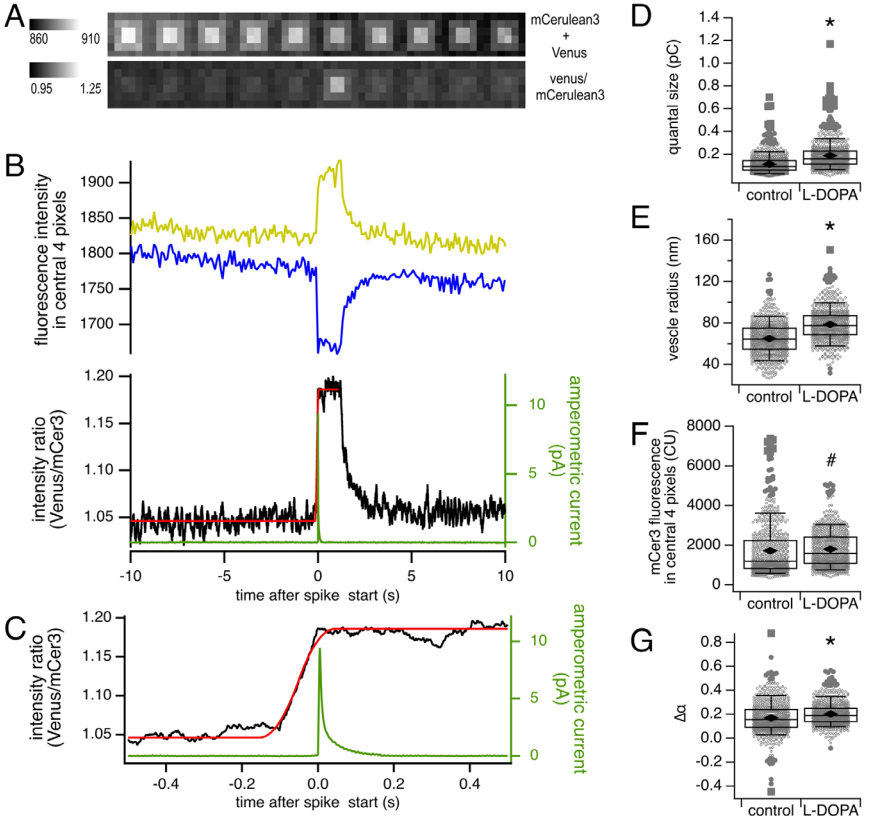

Fig. 6. Increasing vesicle size with L-Dopa treatment increases the fraction of SCORE2 molecules changing conformation. (*A–C*) FRET signals of SCORE2 in L-Dopa loaded cells monitored and analyzed in the same way as shown in Fig. 4. Spatiotemporal correlation between FRET change and fusion is unchanged in L-Dopa-treated cells. (*D–G*), Statistical comparisons between control (657 events from 27 cells) and L-Dopa loaded (671 events from 22 cells) cells. Box plots show Tukey quartiles with whiskers at 9 and 91 percentiles, diamonds indicate mean values. (*D*), Mean vesicle quantal size; (*E*) Cubic roots of quantal size converted to vesicle radius assuming a mean radius of 65 nm for control cells; (*F*), SCORE2 densities at release sites indicated as mCerulean3 fluorescence intensity in the central 4 pixels; (*G*), Average fraction Δα changing from low to high FRET preceding a fusion event. *$P < 0.01$; #$P > 0.05$.

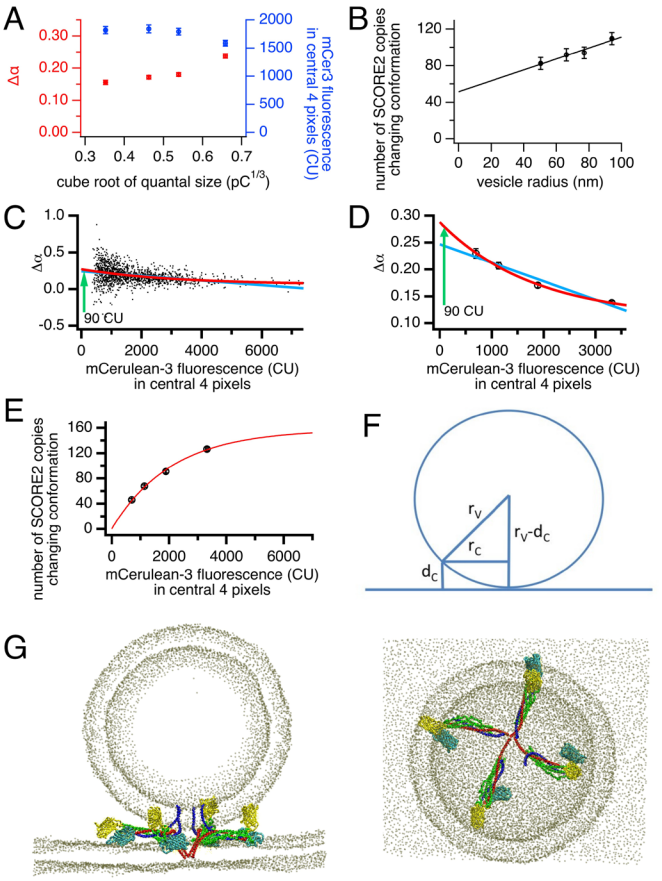

Fig. 7. The number of SCORE2 copies changing conformation increases with vesicle size and SCORE2 density. (*A*) Δα values (red) and SCORE2 densities at fusion sites (blue) plotted vs. cube root of vesicle quantal size. (*B*) Absolute number of SCORE2 copies changing conformation plotted vs. vesicle radius. (*C* and *D*), Plots of Δα vs. corresponding mCerulean3 intensities in central 4 pixels fitted linearly (blue) and exponentially (red). The values of Δα extrapolated to SNAP25 density in wt cells are marked with green arrows. (*C*) Values of individual events; (*D*) Quartile sub-grouped data. (*E*) Number of SCORE2 copies changing conformation vs. mCerulean3 intensity for the grouped data, fitted with the function $\Delta N = \Delta N_{max} \times (1 - \exp(-F_{mCer3}/F_0))$ (red line). (*F*) Model of contact zone between a spherical vesicle and a flat plasma membrane. The model defines the contact zone as the area where the distance between the surface of the sphere and the flat surface is less than the minimum distance for the formation of molecular contacts d_c. For a spherical vesicle with radius r_V the contact zone is a circle with radius r_c with $r_c^2 = 2r_V d_c - d_c^2$ and a contact area $a_c = (2r_V d_c - d_c^2) \times \pi$. (*G*) Snapshot from coarse-grained molecular dynamics simulation of a 40-nm vesicle and planar membrane bridged by 4 SNARE complexes incorporating SCORE2 with calculated FRET efficiency of 41%.

high quartile group to 26% in the low quartile group. Although the density of SCORE2 in the low quartile group is ~4.8 times lower than in the high quartile group, the number of copies changing conformation is only ~2.9 times lower. Linear and exponential fits (Fig. 7*D*) predict $\Delta\alpha_{endogenous}$ of 0.24 and 0.28, respectively. With a corresponding number of ~27 copies of SCORE2 in the 4 pixel area surrounding the fusion site in wt cells, we estimate that 6 to 7 SNAP25 copies undergo a conformational change preceding fusion in wild-type cells. Although Δα decreases somewhat with increasing SCORE2 densities (Fig. 7 *C* and *D*), the estimated absolute number of SCORE2 copies changing conformation ΔN still increases considerably with increasing SCORE2 density (Fig. 7*E*). A fit with the function $\Delta N = \Delta N_{max} \times (1 - \exp(-F_{mCer3}/F_0))$ indicates a maximal value $-N_{max} = 157 \pm 8$, suggesting a limit of ~160 for the maximal number of SCORE2 copies changing conformation before fusion of a vesicle with average size.

Discussion

A FRET-based SCORE incorporating CFP and Venus at the N termini of the SNAP25 SNARE domains SN1 and SN2, respectively, (19) was previously used in bovine chromaffin cells and indicated that a conformational change of SNAP25 precedes individual fusion events precisely at the fusion site (20). Here, we generated an improved version named SCORE2 by replacing CFP with mCerulean3. We expressed this construct in mouse embryonal SNAP25 knock-out chromaffin cells and found that it fully rescues exocytosis in whole cell patch clamp capacitance measurements and that properties of individual release events recorded by carbon fiber amperometry were completely unchanged compared to wild-type cells. SCORE2 is therefore a fully functional substitute for SNAP25. Combining ECI of fusion events using ECD arrays with TIR-FRET imaging, we localized single fusion events and simultaneously tracked the conformational change reported by SCORE2 at the fusion sites.

After localizing vesicle releasing sites using ECI, we find that the fluorescence intensity of SCORE2 at the fusion sites was higher than that in the periphery, confirming the existence of vesicle-associated t-SNARE clusters on the plasma membrane (14). By using the time super-resolution method of Event COrrelation Microscopy (ECOM) (29), we detected an increase of the FRET ratio preceding the onset of the amperometric spike precisely at the fusion site by ~65 ± 11 ms. This delay is similar, albeit slightly shorter than that previously reported when SCORE was expressed in wild-type bovine chromaffin cells. The FRET ratio remained at a plateau for ~1 s and then gradually declined to basal level within ~2 s. At the fusion site, the time course of fluorescence intensity summed from donor and acceptor channels remained constant before and after fusion. The decaying phase of the FRET signal may reflect reversal of the SCORE2 conformational change, or, alternatively, dispersion and exchange of SCORE2 SNARE complexes with uncomplexed SCORE2 molecules after fusion.

The FRET change reported by overexpressed SCORE2 precedes fusion by ~65 ms. Under the conditions of the combined TIR-FRET-ECD experiments, fusion occurs in a sustained manner, activated by the mechanical stimulation of the positioning pipette (20, 25). There is therefore a steady-state cycle of docking and fusion, and the delay suggests that the FRET change likely reflects tight docking and priming of the vesicle, followed by fusion after ~65 ms. This delay is in excellent agreement with the dwell time between vesicle docking and fusion in rod photoreceptors observed under conditions of sustained release as in darkness (34).

The number of SNARE complexes participating in vesicle docking and fusion is highly debated (11, 35). The fact that SCORE2 fully rescues fusion in SNAP25 knock-out cells made it possible to estimate the number of SCORE2 molecules changing conformation before fusion pore opening. By calibration of single-molecule fluorescence, we estimate that on average ~510 SCORE2 molecules were present in the 2 × 2 pixel releasing area of 0.1 μm^2 and ~87 of these (~17%) change conformation during the formation of the tightly docked state at the release site. The number of SCORE2 (or SNAP25 in wt cells) copies that change conformation increases with SNAP25 density at the release site (Fig. 7*E*) and with vesicle size (Fig. 7*B*), suggesting that this number may be related to the number of SNAP25 copies that are present in the vesicle–plasma membrane contact area. A linear relation between the initial docking rate and SNARE density was also found in a reconstituted system of liposomes containing Syb2 at various densities and docking on a t-SNARE doped planar membrane (11). Interestingly, the increase in SNAP25 copies changing conformation during docking does not affect the frequency and properties of the subsequent fusion events (Fig. 2). To engage in a SNARE complex for docking,

SCORE2 must interact with Stx1, which may be recruited from plasma membrane reservoir, and also with Syb2, which is present on the vesicle membrane. The fit of Fig. 7*E* suggests that the number of SCORE2 copies changing conformation increases with its density in the membrane at the fusion site up to ~160. The number of Syb2 copies on a chromaffin granule is unknown. The number of copies on a SV is ~70 (6, 36). The mean diameter of a SV is 42 nm, corresponding to an estimated SV membrane area of 0.00554 μm^2, and an average density of 12,631 VAMP2 copies per μm^2 (36). The mean diameter of mouse embryonal chromaffin cell granules is 130 nm (33), corresponding to an estimated granule membrane area of 0.053 μm^2, nearly 10 times larger than that of SVs. If the surface density of Syb2 in the chromaffin granule membrane were the same as it is in the SV membrane, there would be ~700 copies on a chromaffin granule. The possibility that at very high overexpression 160 SCORE2 copies could potentially interact with a corresponding number of Sybs on the chromaffin granule can thus not be excluded. It is, however, also possible that only a smaller number of SCORE2 copies participate actively in SNARE complex formation and that, as a consequence of the tight docking, additional SCORE2 SNAP25 copies present in the contact zone are squeezed between the vesicle and the plasma membrane, resulting in a tight interaction of the SNAP25 SN1-SN2 SNARE domains.

To estimate the contact zone area, we consider a highly simplified model based on a spherical vesicle on a flat plasma membrane similar to that of (11). The contact zone a_C is defined as the area where the distance d_C between the membrane of the loosely docked or tethered vesicle and the plasma membrane allows for protein interactions that will proceed to the tightly docked, primed state (Fig. 7*F*). The contact zone area a_C in this highly simplified model is

$$a_C = \left(2 \bullet r_V \bullet d_C - d_C^2\right) \bullet \pi. \qquad [5]$$

The radius r_V of an average mouse embryonal chromaffin granule radius is 65 nm (33). This model suggests that the contact zone area and the number molecules within that area, which are able to participate in the docking process, increases linearly with r_V. The number of molecules changing conformation as a function of vesicle radius (Fig. 7*B*) shows indeed a linear relation. The linear regression, however, has an offset value of 53, suggesting the existence of extra copies of SCORE2 at fusion sites participating in the docking process independent of vesicle size. The experimentally determined number of SCORE2 copies (N_D) changing conformation during the transition to the tightly docked state as a function of vesicle radius (Fig. 7*B*) was therefore fitted with the function

$$\begin{aligned} N_D &= \sigma_{SCORE2} \bullet a_C + N_{extra} \\ &= \sigma_{SCORE2} \bullet \left(2 \bullet r_V \bullet d_C - d_C^2\right) \bullet \pi + N_{extra}. \end{aligned} \qquad [6]$$

Here, σ_{SCORE2} is the SCORE2 density in the plasma membrane at fusion sites (~5,100 copies/μm^2 at typical overexpression), and N_{extra} is the number of extra copies, presumably in the cluster present at the fusion site. This fit yields N_{extra} = 57 ± 5 and a contact distance d_C = 19 ± 3 nm. The value of N_{extra} is similar to the number of ~29 ± 4 extra SCORE2 copies in the 4x4 pixel area based on the extra fluorescence associated to the vesicle at the fusion site, suggesting that the extra molecules in the cluster, as well as all additional copies present in the contact zone, change conformation in the docking/priming process. For an average chromaffin granule, the contact zone represents only 7% of the 4 pixel area that was analyzed to include most of the point spread function. For a typical overexpression level with 510 molecules in the 4 pixel area, this corresponds to ~36 molecules plus ~57 extra molecules from the cluster. Out of the 510 molecules, 93% are outside the contact zone and will not interact with the vesicle and therefore not undergo the conformational change that accompanies tight docking.

In wild-type cells, the number of SNAP25 molecules in the 4 pixel 0.1-μm^2 area surrounding the fusion site was thus estimated to be ~27. At this density, the fraction changing conformation preceding fusion is ~26%, and the analysis leads to an estimate of ~6 to 7 SNAP25 molecules undergoing a conformational change during docking in wt cells. Only 2 of the 27 molecules would be present in the vesicle–plasma membrane contact zone. Based on the fit with Eq. **6**, there appears to be a cluster of extra SNAP25 copies that may be associated with the vesicle. For the average high overexpression level of SCORE2, the number N_{extra} is ~57, or 11% of the 510 copies in the 0.1 μm^2 four-pixel area. If this fraction would be the same for the wild-type SNAP25 density, we estimate N_{extra} = 3 (11% of the 27) for a total of 5 copies in the contact area.

Based on cryo-electron tomography (10, 37), chromaffin granules (38–40) as well as SVs (41, 42) are considered (tightly) docked, if they are at a distance of 4 to 5 nm from the plasma membrane and this tightly docked state requires synaptobrevin, syntaxin, and specifically SNAP25 (43). The fit of the data in Fig. 7*B* suggests that all SNAP25 copies present within a ~20-nm vesicle–plasma membrane contact distance change conformation in the transition to this tightly docked state. The value of ~20 nm is consistent with the range where SNARE proteins are able to interact and suggests that these may be the tethered vesicles with vesicle–plasma membrane distance <30 nm (44) undergoing the transition to the tightly docked state. To illustrate how increased FRET may be associated with high FRET in the tightly docked state, we performed simulations in which 4 SNARE complexes bridge a 40 nm vesicle and planar membrane. In these simulations we identified a state with an average FRET efficiency of ~41% from the 4 SNARE complexes. Although FRET values of individual SNARE complexes are highly variable, the snapshots shown in Fig. 7*G* indicate how the transition to the tightly docked primed state may produce a high FRET state.

It is interesting to consider the implications for SVs. It was recently found that SVs are docked by 6 protein complexes, each likely containing one SNARE complex, arranged symmetrically connecting the primed vesicles to the PM (10). In synaptosomes, there is a density of ~11,600 SNAP25 copies per μm^2 (36). With this density, we estimate ~6 copies to be present within a contact distance d_C of 4 nm. Our results suggest that a similar number of SNARE complexes mediates docking of the dense core vesicles in chromaffin cells as of SVs.

Materials and Methods

SCORE2 Probe and Cells. SNAP25$^{-/-}$ knockout mice die at birth. Therefore, SNAP25 knockout mouse E18-E19 embryos were obtained by breeding SNAP25$^{+/-}$ mice and chromaffin cells were cultured as described (33). The appearance of SNAP25$^{-/-}$ embryos is in stark contrast to SNAP25$^{+/-}$ and wt. The SNAP25$^{-/-}$ knockouts exhibit small size, tucked posture, and blotchy skin and lack spontaneous or reflexive movement. The absence of SNAP25 in these embryos was repeatedly confirmed by genotyping. The SCORE2 DNA was modified from the original SCORE plasmid, a kind gift provided by Prof. Wolfhard Almers. Its domain structure was ECFP-linker(GGSGGS)-SNAP25(1-141)-linker(GGSGGS)-Venus-linker(GGSGGS)-SNAP25(142-206) (19). The SCORE2 construct was generated by replacing ECFP in SCORE with mCerulean3, which was performed by mutating multiple residues in ECFP (T62S, S72A, Y145A, S147H, H148G, K166G, I167L, R168N, A206K) and confirmed by DNA sequencing. The SCORE2 DNA was subcloned into a viral vector pSFV1 (Semliki Forest; Invitrogen). The viral transfection was performed 2 d after the cell isolation. The electrophysiological and amperometric measurements were performed ~6 h after the cell transfection. All the experiments were performed at room temperature.

Co-Expression of SCORE2 and Syntaxin-mCherry. SCORE2 and Stx1-mCherry were co-expressed in SNAP25$^{-/-}$ cells. To overexpress Stx1 at a higher level than SCORE2, we introduced an IRES in the pSFV construct, arranging the DNA fragment of Stx1-mCherry upstream IRES and SCORE2 downstream. Stx1a was inserted in the pmCherry-N1 vector (Clontech) at 5′BglII and 3′SalI sites to generate Stx1a-mCherry. The Stx1a-mCherry was PCR amplified to generate 5′ BamHI and 3′ BssHII sites and inserted into the modified pSFV1 vector (GIBCO/BRL), followed by the IRES for co-translation of the SCORE2 protein (45).

Immunocytochemistry of SNAP25. The wt and SNAP25$^{-/-}$ embryonic mice (E18) chromaffin cells were cultured in glass-bottom dishes. On the 2nd day of primary culture, the SNAP25$^{-/-}$ cells were incubated with the pSFV1 construct to overexpress SCORE2 and the expression level of SCORE2 was compared to the endogenous level of SNAP25 in uninfected wt cells. Seven hours after infection, both types of cells were fixed in 4% paraformaldehyde solution for 30 min, permeabilized in 0.1% (v/v) Triton X-100 for 10 min and blocked with 6% bovine albumin serum (Sigma-Aldrich) for 1 h. After removing the blocking buffer, the cells were incubated with the primary mouse anti-SNAP25 antibody (1:2,000, CI 71.1, SYSY) for 2 h, washed 5 times 10 min with PBS, incubated with Alexa Fluor 568–labeled secondary antibodies (Invitrogen, 1:200 dilutions) for 1 h, washed, and mounted. Fluorescence imaging was performed with an Olympus IX83 with UPlsapo 20×/0.75 objective, 561/14 excitation filter, 442/514/561-nm beam splitter and 594-nm long-pass emission filter. Images were acquired with an iXon3 EMCCD camera (Andor Technology) and analyzed using ImageJ.

Electrophysiology. Cell membrane capacitance was recorded using a Patchmaster controlled EPC-10 amplifier (HEKA electronics). The depolarization evoked exocytosis was detected as change in cell capacitance, estimated by the Lindau–Neher technique (21). Membrane capacitance (Cm) changes were analyzed with customized IgorPro routines (WaveMetrics). The standard extracellular solution contained (in mM): 140 mM NaCl, 5 mM KCl, 5 mM $CaCl_2$, 1 mM $MgCl_2$, 10 mM 4-(2-Hydroxyethyl)-1-piperazine ethanesulfonic acid (HEPES)/NaOH, and 20 mM glucose (pH 7.3). The pipette solution contained (in mM): 145 Cesium glutamate, 8 NaCl, 0.18 $CaCl_2$, 0.28 BAPTA, 1 $MgCl_2$, 2 ATP-Mg, 0.5 GTP-Na_2, 0.3 cAMP, 10 HEPES/CsOH (pH 7.3), and 300 nM calculated free $[Ca^{2+}]_i$.

Carbon Fiber Amperometry. Carbon fiber electrodes with a diameter of 5 μm were used for amperometric measurements. Amperometric currents were recorded with the EPC-9 amplifier (HEKA, electronics) applying electrode voltage of 700 mV, filtered at 3 kHz and analyzed by a customized macro for IGOR software (46). The analysis was restricted to events with a peak amplitude >10 pA. To analyze individual amperometric spike and foot parameters, the median values were determined for each individual cell and subsequently averaged over the number of cells (47). Each individual cell provided at least 12 amperometric spikes with at least 5 detectable foot signals. The bath solution contained 140 mM NaCl, 5 mM KCl, 5 mM $CaCl_2$, 1 mM $MgCl_2$, 10 mM HEPES/NaOH, and 20 mM glucose (pH 7.3). Release events were stimulated by applications of high KCl solution: 30 mM NaCl, 100 mM KCl, 5 mM $CaCl_2$, 1 mM $MgCl_2$, 20 mM Glucose, and 10 mM HEPES/NaOH (pH 7.3) for 5 min.

ECD Array Amperometry and Localization of Release Event. The ECD arrays were microfabricated by contact photolithography, patterning four Pt electrodes on a glass coverslip with a space of ~5 μm between them (48). A mouse chromaffin cell expressing SCORE2 was picked up by a micropipette and gently pressed onto this space. Experiments were performed in a solution containing (in mM) 140 NaCl, 5 KCl, 5 $CaCl_2$, 1 $MgCl_2$, 10 HEPES/NaOH, and 20 glucose. Amperometric currents were recorded with a four-channel amplifier (VA-10M4; NPI Electronic), filtered at 500 Hz using the build-in two-pole Bessel filters, and sampled at 1 KHz using a 16-bit analog-to-digital converter (NIDAQ). The amperometric spikes were analyzed using an Igor macro as described (46). The spike starting time was determined by extrapolating the linear fit of the 50 to 90% rising phase back to the baseline.

To modulate the vesicle quantal size, the chromaffin cells were incubated in extracellular solution containing 100 μM L-Dopa for 1 h at 37 °C. The 10 mM L-Dopa stock solution in extracellular solution was freshly prepared before experiments. After incubation, the cells were transferred to the extracellular solution without L-Dopa. The recordings were completed with ~1 h after incubation period.

The vesicle release can be localized by the ECD array, provided that amperometric currents are recorded by at least three electrodes. The molecules discharged from a chromaffin granule have been found to diffuse isotropically in the space between cell membrane and coverslip (49). Different fractions of the molecules will be detected by respective ECD electrodes depending on the location of the release site. Based on the coordinates from the geometrical outline of the electrodes, random work simulations were performed to determine the relation between the release site and the fraction of charges detected by different electrodes. The charges corresponding to the number of molecules detected by each electrode were determined by integrating each amperometric spike. Comparing the measured and simulated fractional charges, the position of fusion events is defined.

Fluorescence Microscopy. Fluorescence imaging was performed with an inverted microscope Olympus IX83 equipped with an Optosplit III (Cairn Research) image splitter fitted with a 509-nm dichroic and emission filters at 467 to 499 nm for the mCerulean3 and 520 to 550 nm for the Venus channel, and with a 565 dichroic and 594 long-pass filter for mCherry and Alexa Fluor 568 emission. For epifluorescence excitation, the set-up was equipped with a Lumen 220 Pro (Prior Scientific) fluorescence lamp with 6 position filter wheel. Illumination in TIRF mode was provided by a 442-nm laser (Changchun New Industries Optoelectronics Tech.Co.).

TIR Fluorescence Microscopy and FRET Measurement in Live Cells. The cell plasma membrane was illuminated in TIRF mode with a 442-nm laser using an Olympus UApo N 1.45 NA 100× oil objective. The fluorescence image was separated with emission filters at 467 to 499 nm for the mCerulean3 and 520 to 550 nm for the Venus channel. The images of the two channels were projected side-by-side onto an EMCCD (Andor iXon3) run by its accompanying software (Solis). For each recording, a 1,000-frame image sequence was collected with 100-ms exposure time and 1.7-ms readout interval such that one frame was acquired every 101.7 ms simultaneously for both channels. The alignment of the blue and yellow images was performed by an algorithm programmed in Igor. The camera provides a TTL signal indicating exposure times that was recorded to synchronize the timing of the fluorescence image frames and electrochemical signals. Unless indicated otherwise, fluorescence intensities are given in CU after background subtraction. The background fluorescence intensity was measured in a region outside the footprint of cells and electrodes.

Fluorescence Calibration of mCerulean3 by Using mCerulean3-SNAP25-His_6/Ni-NTA Beads. To calibrate the fluorescence intensity of single mCerulean3 molecules, mCerulean3-SNAP25-His_6 molecules were coupled to Ni-NTA agarose beads (Qiagen, Cat # 30210). The competent *Escherichia coli* cells (NEB, C3013) were transformed with plasmid DNA containing mCerulean3-SNAP25-His_6. The DNA fragments of 6xHis and mCerulean3 were fused at the C- and N-terminus of SNAP25, respectively. After the growth of the *E. coli* cells containing expression plasmid, the 6xHis-tagged proteins were purified under native conditions. The quantification of purified mCerulean3-SNAP25-His_6 was performed by Coomassie Plus™ Assay (Thermo Scientific). Protein dialysis or desalting was performed to remove ionic or nonionic detergents which interfere with Coomassie-based protein assay. Bovine Serum Albumin (BSA) was utilized as the standard reference protein. A total of 5 dilutions of His_6-tagged mCerulean3-SNAP25 from the stock solution were made in 1ml dilution buffer, covering 0.125×, 0.25×, 0.5×, 1.0×, and 2.0 × 10^{-7}M. The dilution solution contained 300 mM NaCl, 50 mM Tris-HCl, and 1.5 mg/mL BSA, pH 8.0. Then, 30 μL slurry of 50% Ni-NTA agarose beads (Qiagen, Cat # 30210) was added to each sample and the mixtures incubated at 4 °C overnight. According to the beads diameter of 45 ~ 160 μm (provided by the manufacturer), the mean value of total surface area of the beads in each sample was ~9 cm^2. Based on the manufacturing parameters of the beads, the estimated maximal density of mCerulean3-SNAP25-His_6 (~51 kDa) on the bead surface obtained in 2 × 10^{-7}M dilution is 2 × 10^{-7} M × 1 mL × 6 × 10^{23} mol^{-1})/9cm^2 = 1.33 × 10^5 occupied sites/μm^2, which is ~3.3% of the full binding capacity of the beads (~4 × 10^6/μm^2, provided by the manufacturer), such that there is no saturation of binding sites in all samples. The estimated density of mCerulean3-SNAP25-His_6 on the bead surface obtained with the 10^{-7}M incubation is 66,667 molecules/μm^2 or 1,685 molecules per 159-nm pixel (100× objective) with 0.02528-μm^2 pixel area.

Excited at 442 nm in TIRF mode (as in the cell experiments), a central area of the bead-cover slip contact zone was imaged and the average mCerulean3 intensity per pixel determined. The plot of intensity vs. the corresponding incubation concentrations of mCerulean3-SNAP25-His_6 (*SI Appendix*, Fig. S2) is linear with a

slope of 5,700 CU/pixel/10^{-7}M. With the estimate of 1,685 mCerulean3-SNAP25 molecules/pixel/10^{-7}M, this slope yields a calibration factor of 3.38 CU/molecule.

A similar method was previously employed to calibrate Green Fluorescent Protein (GFP) fluorescence (50). In that study, Chiu et al. concluded that at least 85% of the expressed His6-GFP molecules are active as fluorescent molecules. If 15% were inactive as fluorescent molecules in the calibration, the fluorescence per molecule would be underestimated, which would lead to a corresponding overestimate of SCORE2 densities in the plasma membrane by ~15%. Another potential source of error comes from the use of BSA as reference protein for the Coomassie assay that was used to determine mCerulean3-SNAP25-His_6 concentration. The number of Coomassie dye ligands bound to a protein molecule is approximately proportional to the number of positive charges on the protein. The total numbers of positively charged amino acids in BSA and mCerulean3-SNAP25-His_6 are 99 and 63, respectively, which would produce an ~34% lower signal for mCerulean3-SNAP25-His_6 than for BSA if both were present at the same molar concentration. However, BSA and mCerulean3-SNAP25-His_6 have different MW of 66 kDa vs. 51 kDa, respectively. At the same mass/volume concentration, as used in the Coomassie assay, the number of protein molecules per µg protein will thus be ~30% higher for mCerulean3-SNAP25-His_6 and the number of positive charges per µg protein would eventually be ~14% lower than for BSA. If the Coomassie assay signal from mCerulean3-SNAP25-His_6 were in fact 14% lower than for BSA at the same mass/volume concentration, the actual concentration of mCerulean3-SNAP25-His_6 in the calibration with the Ni-NTA beads would be accordingly higher than estimated from the Coomassie assay and the fluorescence per molecule correspondingly lower, increasing our estimates of SCORE2 densities in the plasma membrane accordingly by 14%. This correction would compensate the correction that we estimate from the potential misfolded inactive proteins. Overall, these estimates suggest that our estimates of SCORE2 densities in the plasma membrane are likely not systematically distorted by the calibration method.

Chiu et al. used amino acid analysis for GFP quantification and compared their results also to the Coomassie Plus assay and concluded that the GFP protein concentrations determined with the Coomassie Plus reagent should be multiplied by 0.764 to yield the more accurate concentration. If the same correction were applied to our quantification of SCORE2 concentration, the fluorescence per molecule would be increased and the SCORE2 density estimate would be decreased by ~24%. We conclude that our quantification could possibly overestimate SCORE2 density by ~25%.

In Vitro FRET Measurement. All FRET measurements were performed in a FluoroMax 3 (Horiba Jovin Yvon) spectrometer equipped with a magnetic stirrer. The emission spectra of samples, i.e., SNAP25-SN1 fragment fused mCerulean3 (mCeruSN1), SNAP25-SN2 fragment fused Venus (VenusSN2), SCORE2 only, SCORE2 + Stx1 and SCORE2 + Stx1 + Syb2, were recorded separately at 440-nm excitation with 0.2 s exposure time, optical grating of 1.5 nm for excitation and 3 nm for emission, respectively. In order to quantitatively determine the FRET efficiencies of SCORE2 forming complex with Stx1 or with Stx1+Syb2 by simultaneous spectral unmixing of excitation and emission spectra, the fluorescence intensities of reference samples (mCeruSN1 and VenusSN2), as well as samples of SCORE2 only, SCORE2 + Stx1 and SCORE2 + Stx1 + Syb2 were separately recorded at 200 different emission wavelengths between 400 ~ 600 nm for each of 19 different excitation wavelengths between 380 ~ 570 nm. In the spectral unmixing process, the optical gratings of both excitation and emission were 1nm, and the exposure time was 1 s.

Conversion of Quantal Size to Vesicle Radius. Quantal size Q (in pC) is proportional to vesicle volume V_V with a constant vesicular catecholamine concentration C_V (32), $Q = 2 \bullet F \bullet C_V \bullet V_V$, where F is Faradays constant. The factor 2 comes from the fact that 2 electrons are transferred during oxidation of 1 catecholamine molecule. Vesicle radius is therefore proportional to $Q^{1/3}$. Mean radius of mouse embryonal chromaffin granules is 65 nm (33) and mean $Q^{1/3}$ in our experiments without L-Dopa was 0.455 $pC^{1/3}$, such that R_V of an individual vesicle can be estimated as $R_V = \frac{Q^{1/3}}{0.455\ pC^{1/3}} \bullet 65$ nm. This relation corresponds to a vesicular catecholamine concentration C_V of ~425 mM.

Molecular Dynamics Simulations. The model of the initial SNARE complex structure based on PDB entry 3HD7 and missing residues added as described (51). Briefly, the missing C-terminal residues T116 of Syb2, F287–G288 of Stx1, and K201–G206 of SNAP25 were added using Modeller (52). The SNAP25 linker region residues K83 to A100 (KFCGLCVCPCNKLKSSDA) were added assigning a random coil secondary structure, using I-TASSER server (53). The complete model of SCORE2 was generated using Modeller by adding the fluorescent proteins with GGSGGS or GGSGGSGGSGGS as linkers between the fluorescent proteins and SNAP25. The FRET donor was added at the N-terminus and was modeled based on the crystal structure of Cerulean fluorescent protein (PDB ID: 2WSO). The acceptor fluorophore was based on the atomistic structure of Venus yellow fluorescent protein (PDB ID: 1MYW) and inserted between the SNAP25 linker and the helical SNAP25 SN2 domain. The atomistic structures were converted to coarse-grained models defined by MARTINI force-field (54). For simulation of the vesicle-planar membrane system bridged by 4 SNARE complexes incorporating SCORE2, the initial, pre-equilibrated setup of 40-nm vesicle-membrane system with four syb2-stx-SNAP25 complexes was taken from our previous study (51). In this system, each SNAP25 was replaced by the SCORE2 model described above.

Tracking Donor-Acceptor Distance, κ^2, and FRET Efficiency during MD Simulation. The Förster radius to the sixth power (R_0^6) depends on the fluorescence quantum yield of the donor in the absence of acceptor, the spectral overlap, the molar extinction coefficient of the acceptor, the normalized emission spectrum of the donor, the refractive index n (1.37 for cells) and the dipole orientation factor κ^2. During the simulation, the fluorescent proteins tumble slowly, compared to the fluorescence lifetime such that the assumption of dynamic orientation averaging ($\kappa^2 = 2/3$) is not valid. We therefore determined the value of R_0^6 of the mCerulean3-mVenus pair for $\kappa^2 = 1$ to be 50167179723 Å^6 using https://www.fpbase.org/fret/ and calculated for each state in the simulations the actual R_0^6 values as $R_0^6 = 50{,}167{,}179{,}723$ Å$^6 \times \kappa^2$.

The transition dipole moment (TDM) of the donor and acceptor chromophore was defined as a vector along the backbone beads of residues 111 and 147, as this vector overlapped with the TDM of the chromophore. The residue numberings refer to the respective crystal structures of the fluorophores. The distance between the two fluorophores was defined as distance between backbone beads of the tyrosines at the site of the chromophore (*SI Appendix*, Fig. S3). The orientation factor k^2 was then calculated using the following relation:

$$\kappa^2 = \left(sin\theta_D \bullet sin\theta_A \cdot cos\phi - 2cos\theta_D \bullet cos\theta_A\right)^2.$$

For definition of angles, see *SI Appendix*, Fig. S3.

Data, Materials, and Software Availability. All study data are included in the article and/or *SI Appendix*.

ACKNOWLEDGMENTS. We are grateful to Erwin Neher for continued support and Wolfhard Almers for critical reading and comments and also Federica Castellani for comments on the manuscript. This work has been supported by European Research Council grant ADG 322699 and US NIH grants R01GM121787 and R35GM139608.

Author affiliations: [a]Nanoscale Cell Biology, Max-Planck-Institute for Biophysical Chemistry, Göttingen D-37077, Germany; [b]Science for Life Laboratory, Department of Cell and Molecular Biology, Uppsala University, Uppsala 75124, Sweden; [c]Department of Neurobiology, Max-Planck-Institute for Biophysical Chemistry, Göttingen D-37077, Germany; and [d]Department of Physiology and Biophysics, University of Miami School of Medicine, Miami, FL 33136

1. J. E. Rothman, The protein machinery of vesicle budding and fusion. *Protein Sci.* **5**, 185–194 (1996).
2. R. Jahn, R. H. Scheller, SNAREs–Engines for membrane fusion. *Nat. Rev. Mol. Cell Biol.* **7**, 631–643 (2006).
3. T. Weber *et al.*, SNAREpins: Minimal machinery for membrane fusion. *Cell* **92**, 759–772 (1998).
4. N. Takahashi *et al.*, SNARE conformational changes that prepare vesicles for exocytosis. *Cell Metab.* **12**, 19–29 (2010).
5. M. B. Jackson, SNARE complex zipping as a driving force in the dilation of proteinaceous fusion pores. *J. Membr. Biol.* **235**, 89–100 (2010).
6. S. Takamori *et al.*, Molecular anatomy of a trafficking organelle. *Cell* **127**, 831–846 (2006).

7. T. C. Sudhof, Neurotransmitter release: The last millisecond in the life of a synaptic vesicle. *Neuron* **80**, 675–690 (2013).
8. R. Sinha, S. Ahmed, R. Jahn, J. Klingauf, Two synaptobrevin molecules are sufficient for vesicle fusion in central nervous system synapses. *Proc. Natl. Acad. Sci. U.S.A.* **108**, 14318–14323 (2011).
9. R. Mohrmann, H. de Wit, M. Verhage, E. Neher, J. B. Sorensen, Fast vesicle fusion in living cells requires at least three SNARE complexes. *Science* **330**, 502–505 (2010).
10. A. Radhakrishnan *et al.*, Symmetrical arrangement of proteins under release-ready vesicles in presynaptic terminals. *Proc. Natl. Acad. Sci. U.S.A.* **118**, e2024029118 (2021).
11. J. M. Hernandez, A. J. Kreutzberger, V. Kiessling, L. K. Tamm, R. Jahn, Variable cooperativity in SNARE-mediated membrane fusion. *Proc. Natl. Acad. Sci. U.S.A.* **111**, 12037–12042 (2014).
12. H. Mostafavi *et al.*, Entropic forces drive self-organization and membrane fusion by SNARE proteins. *Proc. Natl. Acad. Sci. U.S.A.* **114**, 5455–5460 (2017).
13. J. J. Sieber *et al.*, Anatomy and dynamics of a supramolecular membrane protein cluster. *Science* **317**, 1072–1076 (2007).
14. M. K. Knowles *et al.*, Single secretory granules of live cells recruit syntaxin-1 and synaptosomal associated protein 25 (SNAP-25) in large copy numbers. *Proc. Natl. Acad. Sci. U.S.A.* **107**, 20810–20815 (2010).
15. N. R. Gandasi, S. Barg, Contact-induced clustering of syntaxin and munc18 docks secretory granules at the exocytosis site. *Nat. Commun.* **5**, 3914 (2014).
16. A. Pertsinidis *et al.*, Ultrahigh-resolution imaging reveals formation of neuronal SNARE/Munc18 complexes in situ. *Proc. Natl. Acad. Sci. U.S.A.* **110**, E2812–E2820 (2013).
17. C. Ma, W. Li, Y. Xu, J. Rizo, Munc13 mediates the transition from the closed syntaxin-Munc18 complex to the SNARE complex. *Nat. Struct. Mol. Biol.* **18**, 542–549 (2011).
18. H. Sakamoto *et al.*, Synaptic weight set by Munc13-1 supramolecular assemblies. *Nat. Neurosci.* **21**, 41–49 (2018).
19. S. J. An, W. Almers, Tracking SNARE complex formation in live endocrine cells. *Science* **306**, 1042–1046 (2004).
20. Y. Zhao *et al.*, Rapid structural change in synaptosomal-associated protein 25 (SNAP25) precedes the fusion of single vesicles with the plasma membrane in live chromaffin cells. *Proc. Natl. Acad. Sci. U.S.A.* **110**, 14249–14254 (2013).
21. M. Lindau, E. Neher, Patch-clamp techniques for time-resolved capacitance measurements in single cells. *Pfluegers Arch./Eur. J. Physiol.* **411**, 137–146 (1988).
22. R. H. Chow, L. v. Rüden, E. Neher, Delay in vesicle fusion revealed by electrochemical monitoring of single secretory events in adrenal chromaffin cells. *Nature* **356**, 60–63 (1992).
23. A. Albillos *et al.*, The exocytotic event in chromaffin cells revealed by patch amperometry. *Nature* **389**, 509–512 (1997).
24. L. W. Gong, G. A. de Toledo, M. Lindau, Exocytotic catecholamine release is not associated with cation flux through channels in the vesicle membrane but Na^+ influx through the fusion pore *Nat. Cell Biol.* **9**, 915–922 (2007).
25. A. F. Dias *et al.*, An electrochemical detector array to study cell biology on the nanoscale. *Nanotechnology* **13**, 285–289 (2002).
26. I. Hafez *et al.*, Electrochemical imaging of fusion pore openings by electrochemical detector arrays. *Proc. Natl. Acad. Sci. U.S.A.* **102**, 13879–13884 (2005).
27. S. S. Rathore, M. Huang, Y. Zhao, Q. Fang, M. Lindau, "Electrochemical imaging of exocytotic fusion events using electrochemical detector arrays" in *Compendium of In Vivo Monitoring in Real-Time Molecular Neuroscience*, G. S. Wilson, A. C. Michael, Eds. (World Scientific Publishing Co, Singapore, 2020), pp. 91–107.
28. J. B. Sorensen *et al.*, Differential control of the releasable vesicle pools by SNAP-25 splice variants and SNAP-23. *Cell* **114**, 75–86 (2003).
29. Q. Fang, Y. Zhao, M. Lindau, Precise time superresolution by event correlation microscopy. *Biophys. J.* **116**, 1732–1747 (2019).
30. S. Mustafa, J. Hannagan, P. Rigby, K. Pfleger, B. Corry, Quantitative Forster resonance energy transfer efficiency measurements using simultaneous spectral unmixing of excitation and emission spectra. *J. Biomed. Opt.* **18**, 26024 (2013).
31. T. L. Colliver, S. J. Pyott, M. Achalabun, A. G. Ewing, VMAT-Mediated changes in quantal size and vesicular volume. *J. Neurosci.* **20**, 5276–5282 (2000).
32. L. W. Gong, G. Alvarez De Toledo, M. Lindau, Secretory vesicles membrane area is regulated in tandem with quantal size in chromaffin cells. *J. Neurosci.* **23**, 7917–7921 (2003).
33. M. Borisovska *et al.*, v-SNAREs control exocytosis of vesicles from priming to fusion. *EMBO J.* **24**, 2114–2126 (2005).
34. M. Chen, M. J. Van Hook, D. Zenisek, W. B. Thoreson, Properties of ribbon and non-ribbon release from rod photoreceptors revealed by visualizing individual synaptic vesicles. *J. Neurosci.* **33**, 2071–2086 (2013).
35. Y. Zhang, L. Ma, H. Bao, Energetics, kinetics, and pathways of SNARE assembly in membrane fusion. *Crit. Rev. Biochem. Mol. Biol.* **57**, 443–460 (2022).
36. B. G. Wilhelm *et al.*, Composition of isolated synaptic boutons reveals the amounts of vesicle trafficking proteins. *Science* **344**, 1023–1028 (2014).
37. G. F. Kusick, T. H. Ogunmowo, S. Watanabe, Transient docking of synaptic vesicles: Implications and mechanisms. *Curr. Opin. Neurobiol.* **74**, 102535 (2022).
38. R. Mohrmann *et al.*, Synaptotagmin interaction with SNAP-25 governs vesicle docking, priming, and fusion triggering. *J. Neurosci.* **33**, 14417–14430 (2013).
39. K. N. Man *et al.*, Identification of a Munc13-sensitive step in chromaffin cell large dense-core vesicle exocytosis. *elife* **4**, e10635 (2015).
40. B. Tawfik *et al.*, Synaptotagmin-7 places dense-core vesicles at the cell membrane to promote Munc13-2- and Ca(2+)-dependent priming. *elife* **10**, e64527 (2021).
41. C. Imig *et al.*, The morphological and molecular nature of synaptic vesicle priming at presynaptic active zones. *Neuron* **84**, 416–431 (2014).
42. S. Chang, T. Trimbuch, C. Rosenmund, Synaptotagmin-1 drives synchronous Ca(2+)-triggered fusion by C2B-domain-mediated synaptic-vesicle–membrane attachment. *Nat. Neurosci.* **21**, 33–40 (2018).
43. C. Papantoniou *et al.*, Munc13- and SNAP25-dependent molecular bridges play a key role in synaptic vesicle priming. *Sci. Adv.* **9**, eadf6222 (2023).
44. S. Watanabe *et al.*, Ultrafast endocytosis at Caenorhabditis elegans neuromuscular junctions. *Elife* **2**, e00723 (2013).
45. D. E. Knight, Secretion from bovine chromaffin cells acutely expressing exogenous proteins using a recombinant Semliki Forest virus containing an EGFP reporter. *Mol. Cell Neurosci.* **14**, 486–505 (1999).
46. E. V. Mosharov, D. Sulzer, Analysis of exocytotic events recorded by amperometry. *Nat. Methods* **2**, 651–658 (2005).
47. T. L. Colliver, E. J. Hess, E. N. Pothos, D. Sulzer, A. G. Ewing, Quantitative and statistical analysis of the shape of amperometric spikes recorded from two populations of cells. *J. Neurochem.* **74**, 1086–1097 (2000).
48. K. Berberian, K. Kisler, Q. Fang, M. Lindau, Improved surface-patterned platinum microelectrodes for the study of exocytotic events. *Anal. Chem.* **81**, 8734–8740 (2009).
49. J. A. Steyer, H. Horstmann, W. Almers, Transport, docking and exocytosis of single secretory granules in live chromaffin cells. *Nature* **388**, 474–478 (1997).
50. C. S. Chiu, E. Kartalov, M. Unger, S. Quake, H. A. Lester, Single-molecule measurements calibrate green fluorescent protein surface densities on transparent beads for use with "knock-in" animals and other expression systems. *J. Neurosci. Methods* **105**, 55–63 (2001).
51. S. Sharma, M. Lindau, Molecular mechanism of fusion pore formation driven by the neuronal SNARE complex. *Proc. Natl. Acad. Sci. U.S.A.* **115**, 12751–12756 (2018).
52. B. Webb, A. Sali, Comparative protein structure modeling using MODELLER. *Curr. Protoc. Bioinf.* **54**, 37 (2016).
53. A. Roy, A. Kucukural, Y. Zhang, I-TASSER: A unified platform for automated protein structure and function prediction. *Nat. Protoc.* **5**, 725–738 (2010).
54. S. J. Marrink, H. J. Risselada, S. Yefimov, D. P. Tieleman, A. H. de Vries, The MARTINI force field: Coarse grained model for biomolecular simulations. *J. Phys. Chem. B* **111**, 7812–7824 (2007).